jmb Article

Membrane-Dependent Conformation, Dynamics, and Lipid Interactions of the Fusion Peptide of the Paramyxovirus PIV5 from Solid-State NMR

Hongwei Yao and Mei Hong

Department of Chemistry, *Iowa State University, Ames, IA 50011, USA*

Correspondence to Mei Hong: *mhong@iastate.edu*
http://dx.doi.org/10.1016/j.jmb.2012.11.027
Edited by A. G. Palmer III

Abstract

The entry of enveloped viruses into cells requires protein-catalyzed fusion of the viral and cell membranes. The structure–function relation of a hydrophobic fusion peptide (FP) in viral fusion proteins is still poorly understood. We report magic-angle-spinning solid-state NMR results of the membrane-bound conformation, dynamics, and lipid interactions of the FP of the F protein of the paramyxovirus, parainfluenza virus 5 (PIV5). ^{13}C chemical shifts indicate that the PIV5 FP structure depends on the composition of the phospholipid membrane: the peptide is α-helical in palmitoyloleoylphosphatidylglycerol-containing anionic membranes but mostly β-sheet in neutral phosphocholine membranes. Other environmental factors, including peptide concentration, cholesterol, membrane reconstitution protocol, and a Lys solubility tag, do not affect the secondary structure. The α-helical and β-sheet states exhibit distinct dynamics and lipid interactions. The β-sheet FP is immobilized, resides on the membrane surface, and causes significant membrane curvature. In contrast, the α-helical FP undergoes intermediate-timescale motion and maintains the lamellar order of the membrane. Two-dimensional ^{31}P–^{1}H correlation spectra show clear ^{31}P–water cross peaks for anionic membranes containing the α-helical FP but weak or no ^{31}P–water cross peak for neutral membranes containing the β-sheet FP. These results suggest that the β-sheet FP may be associated with high-curvature dehydrated fusion intermediates, while the α-helical state may be associated with the extended prehairpin state and the post-fusion state. Conformational plasticity is also a pronounced feature of the influenza and human immunodeficiency virus FPs, suggesting that these Gly-rich sequences encode structural plasticity to generate and sense different membrane morphologies.

Introduction

The generation of membrane curvature underlies many biological processes such as virus entry into cells,[1,2] virus budding,[3,4] pore formation by antimicrobial peptides,[5–7] and membrane vesicularization.[8,9] One of the most studied membrane deformation events is the entry of enveloped viruses into cells, in which fusogenic proteins of the viruses catalyze the merger of the viral membrane and the cell membrane by undergoing a series of large conformational changes.[1,2] Figure 1a illustrates the fusion model that has been proposed for class I viral fusion proteins such as the influenza virus hemagglutinin (HA), the human immunodeficiency virus (HIV) env, and the paramyxovirus F protein. In the pre-fusion state, the trimeric protein has a globular head that is anchored to the virus envelope by a C-terminal hydrophobic transmembrane (TM) domain. Sequestered inside this globular head is a second hydrophobic domain called the fusion peptide (FP). Primed by proteolytic cleavage at the N-terminus of the FP domain and activated by low pH or binding of another viral protein to cell-surface receptors, the protein undergoes dramatic refolding. It first changes to an extended intermediate that exposes the FP and inserts it into the target cell membrane, then bends back onto itself to form a helical hairpin, in which two heptad-repeat domains zip up along each other, in so doing pulling the viral and target membranes together. During these

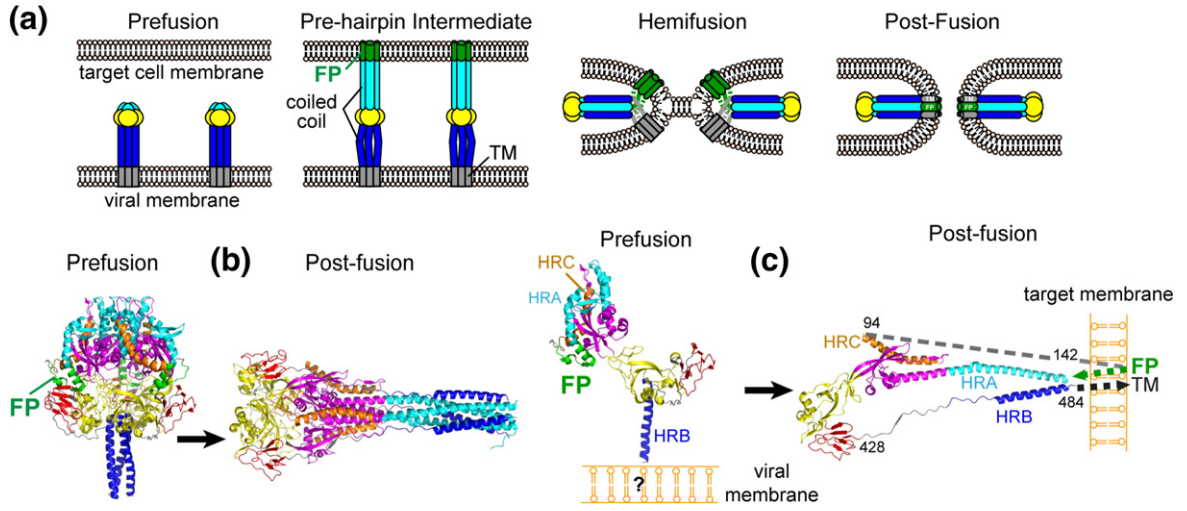

Fig. 1. Model of viral cell membrane fusion by class I fusion proteins. (a) Schematic diagrams of the hypothesized structural transformations of the fusion protein and lipid membranes during fusion. The FP and TM domains are shown in green and gray, respectively. (b) Pre- and post-fusion crystal structures of the trimeric F protein of the parainfluenza virus.[13,14] The structures are oriented to match the schematic pre- and post-fusion protein orientations in (a). (c) Monomer view of the pre- and post-fusion structures of the F protein. The positions of the viral and cell membranes are hypothetical. In the pre-fusion state, the location of the putative TM domain is indicated by a question mark. In the post-fusion structure, broken lines indicate the region of missing electron densities, which include the FP and TM domains. HRA and HRB are heptad-repeat domains.

protein conformational changes, the two lipid membranes also presumably transition through various intermediates such as lipid stalk and hemifusion, which involve high membrane curvature and dehydration of the inter-membrane space.[10,11] Eventually, the viral and cell membranes fuse into a single membrane, in which the FP and TM domains lie in close proximity, constrained by the six-helix bundle formed by the two water-soluble heptad repeats within each monomer of the trimer.

This conceptual framework of viral membrane fusion results from extensive X-ray crystallographic and electron microscopy studies of the structures of the water-soluble part of the fusion proteins in the pre- and post-fusion states.[1,2,12–14] However, the structures of the membrane-bound FP and TM domains are still poorly understood, leaving significant gaps in our understanding of the mechanism of membrane fusion. Except for the pre-fusion state, in which the FP is sequestered in the globular head, the membrane-bound states of FP and TM have not been detected in the crystal structures due to either exclusion of these sequences from the protein construct or a lack of electron density for these segments[13,14] (Fig. 1b). Thus, mechanistic models about the role of FP and TM domains during fusion remain hypothetical. Extensive studies using NMR and electron paramagnetic resonance spectroscopy provided some of the missing information for the FPs of influenza virus and HIV[15–18] and showed that both FPs have significant conformational plasticity, influenced by environmental factors such as peptide concentration and membrane composition. Low peptide concentrations and detergent micelles tend to promote an α-helical structure,[16–18] while high peptide concentrations and cholesterol-rich bilayers mimicking the viral envelopes tend to promote a β-sheet conformation.[19–21] In addition to the secondary structure, the depth of insertion of FPs has been investigated using NMR and infrared (IR) spectroscopy. The fusion-active β-sheet form of the HIV FP is inserted into the center of the lipid bilayer[22] whereas the α-helical influenza FP is obliquely inserted.[16,23] However, how the different FP structures relate to the lipidic intermediates of the fusion pathway and how FPs coordinate with the water-soluble domain to catalyze fusion remain unknown.

To elucidate the mechanism of viral membrane fusion, here we employ magic-angle-spinning (MAS) solid-state NMR (SSNMR) spectroscopy to investigate the structure and membrane interaction of the FP of the parainfluenza virus 5 (PIV5) F protein. We measure the FP backbone conformation as a function of membrane composition and correlate it with several structural observables, including peptide backbone dynamics, depth of insertion into the membrane, peptide-induced membrane morphology, and membrane hydration. We find that, similar to the HIV and influenza FPs, the PIV5 FP is pleomorphic, and correlation of the above panel of structural information suggests an assignment of the different peptide secondary structures to distinct fusion intermediates.

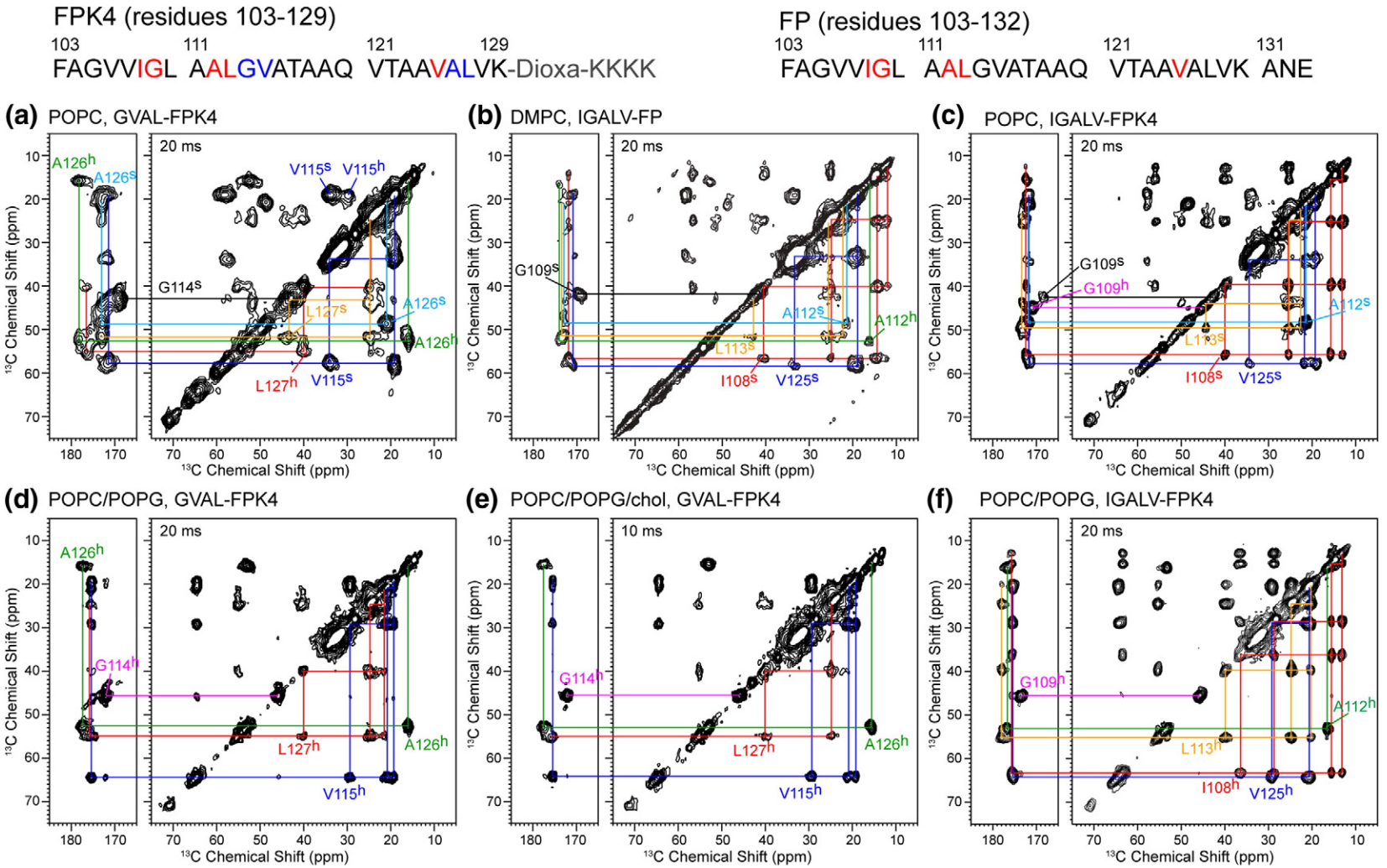

Fig. 2. 2D ^{13}C–^{13}C MAS correlation spectra of the PIV5 FP in gel-phase lipid membranes. The amino acid sequences of FPK4(103–129) and FP(103–132) are shown at the top. The positions of the labeled residues are indicated in blue for GVAL and in red for IGALV. (a) GVAL-FPK4 in POPC (organic) bilayers. (b) IGALV-FP in DMPC bilayers. (c) IGALV-FPK4 in POPC bilayers. (d) GVAL-FPK4 in POPC/POPG bilayers. (e) GVAL-FPK4 in POPC/POPG/cholesterol bilayers. (f) IGALV-FPK4 in POPC/POPG bilayers. Assignments are shown with superscripts s for β-sheet and h for α-helix conformations. The spectra in (b)–(f) were measured at 243 K and the spectrum in (a) was measured at 263 K. In anionic membranes (d–f), only α-helical chemical shifts were observed; in neutral membranes, β-sheet chemical shifts were observed for most residues, while some residues also showed a second set of helical chemical shifts.

Results

Conformation and dynamics of PIV5 FP in different lipid membranes

We measured the ^{13}C chemical shifts of site-specifically labeled PIV5 FP under different conditions to determine how the membrane composition and membrane reconstitution protocol affect the peptide conformation. To increase the solubility of the peptide, we added a KKKK tag to the C-terminus through a DIOXA (8-amino-3,6-dioxaoctanic acid) linker. The tagged FP(103–129) is called FPK4 to distinguish it from the untagged FP(103–132) (Fig. 2). The Lys tag significantly increased the solubility of the peptide in both organic and aqueous solutions. The potential effect of the Lys tag on the peptide conformation was examined. We prepared most proteoliposome samples by first mixing the peptide and lipids in organic solvents. This ensures complete solubilization and homogeneous mixing of the peptide and lipids and prevents artifactual conformations of the peptide due to low-solubility-induced aggregation. Two ^{13}C, ^{15}N-labeled peptides (G114, V115, A126, L127 and I108, G109, A112, L113, V125) were studied, with the labeled positions spanning both the N- and C-terminal halves of the sequence to obtain a global view of the peptide conformation. The ^{13}C chemical shifts were measured in the gel phase of the membranes to suppress potential intermediate-timescale motion and increase the signal sensitivity. Comparison of the one-dimensional (1D) ^{13}C spectra at low and high temperatures (Fig. 4) indicated no change in the chemical shifts or peptide conformation between the gel phase and liquid-crystalline phase.

Figure 2 shows the two-dimensional (2D) ^{13}C–^{13}C MAS correlation spectra of various bilayer-bound PIV5 FPs. In neutral palmitoyloleoylphosphatidylcholine (POPC) and dimyristoylphosphatidylcholine (DMPC) bilayers, some residues (G109, A112, V115, A126, and L127) exhibit a mixture of β-sheet and α-helical chemical shifts while other residues (I108, L113, G114, and V125) show only β-sheet chemical shifts. For most mixed-conformation residues, the helix and sheet percentages are similar based on cross peak intensities (Table S1), except for V115, whose helix fraction is only about 24%. The mixed conformation is observed for both the Lys-tagged FPK4(103–129) and the untagged FP(103–132) (Fig. 2a and b), indicating that the solubility tag does not perturb the peptide conformation.

We also assessed the conformational dependence of the PIV5 FP on the amount of aqueous solution used during membrane reconstitution. For most samples, after the peptides and lipids were mixed in organic solvents, the dried mixtures were subjected to dialysis before being spun down to yield the membrane pellets. We call these samples "aqueous" samples because of the exposure of the proteoliposomes to large volumes of aqueous solution. However, for one POPC sample, the peptide–lipid mixture was directly hydrated with the desired amount of buffer in the NMR rotor. This sample is called the "organic" sample. 1D double-quantum (DQ) filtered ^{13}C spectra without lipid ^{13}C signals (Fig. S1) show that this organic FPK4/POPC sample has the same mixed helix/sheet chemical shifts as the aqueous FPK4/POPC sample, although the percentage of the helical conformation is moderately higher for the organic sample. Thus, the PIV5 FP secondary structure is largely independent of the amount of aqueous solution during membrane reconstitution.

In contrast to the mixed helix/sheet conformation in phosphocholine (PC) membranes, in palmitoyloleoylphosphatidylglycerol (POPG)-containing anionic membranes with or without cholesterol, all nine labeled residues showed predominantly α-helical chemical shifts (Fig. 2d–f). The ^{13}C chemical shift differences from the neutral membrane situation are further captured in the 1D DQ filtered spectra (Fig. S1).

To determine whether the residues that exhibit only β-sheet signals in the neutral PC membrane (I108, L113, G114, V115) (Fig. 2a–c) have a second population of α-helical conformation that may be invisible due to intermediate-timescale motion, we analyzed the C^{α}–C^{β} cross peak intensities of non-Gly residues in the 2D spectra. The spectra of the helical FPK4 in anionic membranes indicate that the Ala C^{α}–C^{β} peak is 2-fold higher than the Val, Leu, and Ile C^{α}–C^{β} peaks due to the higher cross-polarization (CP) efficiency of the Ala methyl carbon. Similarly, the β-sheet signals of I108 and V125 are 40–55% of the total intensities of the mixed-conformation A112 and A126 signals. Therefore, there is no significant amount of dynamically invisible α-helical conformation for these Val and

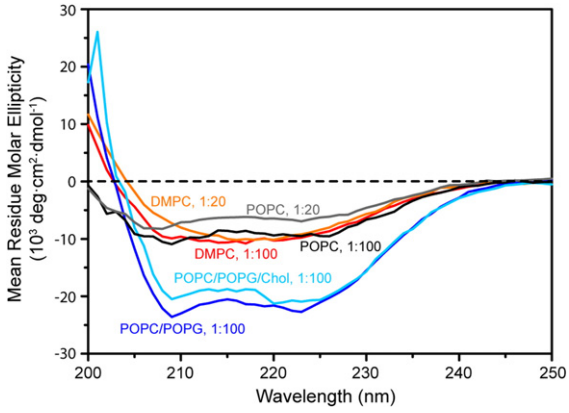

Fig. 3. CD spectra of PIV5 FP in different lipid membranes and P/L ratios of 1:100 and 1:20.

Ile residues. The one exception is L113, whose β-sheet intensity is only ~20% of the total A112 intensity, suggesting dynamic disorder at L113 even at 243 K. Taken together, these data indicate that two FP populations exist in the PC membrane: one with a predominantly β-sheet conformation while the other with mixed helix/sheet conformations.

The conformation-dependent ^{13}C chemical shifts were measured at relatively high P/L (*p*eptide/*l*ipid) ratios of 1:13 to 1:20. To evaluate if lower peptide concentrations change the secondary structure, we measured the circular dichroism (CD) spectra of FPK4 at P/L = 1:100 (Fig. 3). Ellipticities below 200 nm were not measured due to light scattering from the lipid vesicles; thus, we focus on the ellipticities between 200 nm and 250 nm. For POPC/POPG/cholesterol and POPC/POPG membranes with a P/L of 1:100, clear minima were observed at 209 nm and 223 nm, indicating a dominant α-helical conformation. In contrast, in neutral POPC and DMPC membranes, the peptide shows no double minima but stronger negative intensities at ~216 nm, which are characteristic of β-sheet structures. Thus, the helical content of the peptide is significantly reduced in the neutral membranes. Spectral deconvolution indicates that FPK4 has a helicity of about 75 ± 10% in anionic membranes but only 30 ± 10% in POPC and DMPC membranes (Table S2). Since low P/L (down to 1:100) did not change the peptide conformation to α-helix in the neutral membrane, these data indicate that the β-sheet conformation is an intrinsic property of the FP in the zwitterionic membrane rather than a result of low-solubility-induced peptide aggregation before membrane binding. FPK4 did not form homogeneous suspensions with anionic lipid membranes at a high P/L of 1:20. This suggests that the α-helical FP caused large membrane aggregates that precipitated out of the solution.

To determine whether the mobility of the PIV5 FP differs between the α-helical and β-sheet states, we measured the 1D ^{13}C CP MAS spectra as a function of temperature. The β-sheet signals of POPC-bound FPK4 (Fig. 4a) are relatively insensitive to temperature from 253 K to 303 K, indicating that the peptide is immobilized by oligomerization. Quantitative C–H order parameters confirmed the immobile nature of the β-sheet peptide: the C–H dipolar dephasing curves of DMPC- and POPC-bound FP and FPK4 show C^{α}–H^{α} order parameters of 0.87–0.97 (Fig. S2 and Table S3). The POPC-bound FPK4 showed larger T_2 decays in the dipolar dephasing curves than the DMPC-bound FP, indicating that the lower phase transition temperature of the POPC bilayer caused more pronounced intermediate-timescale motion of the peptide.[24] In contrast, the ^{13}C signals of POPC/POPG-bound FPK4 are significantly broadened between 273 K and 313 K, preventing the measurement of well-resolved ^{13}C spectra (Fig. 4b). Temperature-dependent spectral broadening has been

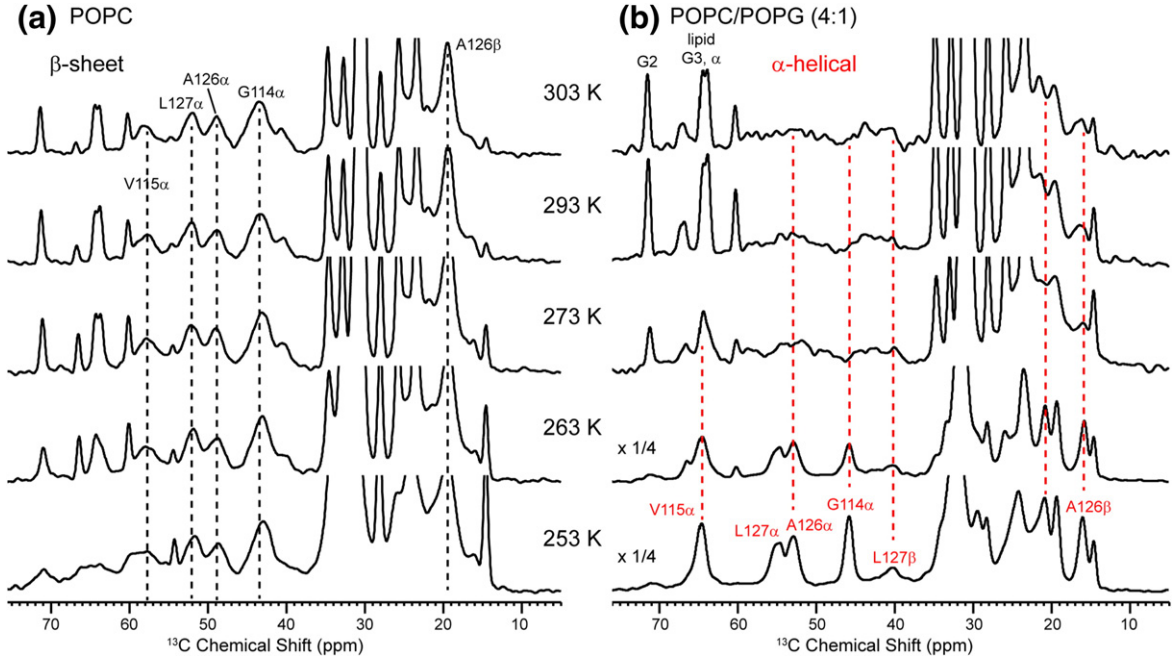

Fig. 4. Variable-temperature (253–303 K) ^{13}C CP MAS spectra of GVAL-FPK4 bound to different membranes. (a) POPC membrane. The chemical shifts, linewidths, and intensities of the β-sheet peptide are insensitive to temperature, indicating that the FP is immobilized in the POPC membrane at ambient temperature. (b) POPC/POPG membrane. The signals of the α-helical FPK4 broaden above 273 K, indicating intermediate-timescale motion. The sharp signals in the 60- to 70-ppm range above 273 K result from the lipids.

observed in a number of membrane peptides[25–27] and results from lipid-bilayer-induced intermediate-timescale motion of the peptides. For example, the ^{13}C MAS signals of dilauroylphosphatidylcholine- and POPC-bound influenza M2 transmembrane peptide (M2TM) are broadened beyond detection at 293 K but become well resolved again at 313 K due to fast uniaxial diffusion of the helical bundle.[25,28] In contrast, the PIV5 FP is unable to increase its motional rate to the fast regime by 313 K, indicating that the membrane-bound structure of this FP prevents fast motion even at physiological temperature.

Depth of insertion of the PIV5 FP

We investigated the depth of insertion of the FP using the 2D ^{13}C-detected ^{1}H spin diffusion experiment, which correlates the lipid CH_2 and water ^{1}H signals with the peptide ^{13}C signals[29] in the liquid-crystalline phase of the membrane. The experiment requires the peptide or protein to be immobilized to distinguish it from the mobile lipids and water. Since the signals of the helical FP are broadened by motion at ambient experiment, only the depth of the β-sheet peptide can be determined in this way. The spectra of DMPC-bound FP show no lipid–peptide cross peaks even at a mixing time of 900 ms (Fig. 5a–c), indicating that the β-sheet peptide lies on the membrane surface, out of spin diffusion reach of the lipid acyl chains. Our previous study of anionic DNA bound to cationic dioleoyltrimethylammonium-propane bilayers showed lipid–DNA cross peaks by 900 ms,[29] even though DNA cannot insert into the middle of the cationic lipid bilayer.[30] Thus, subtle distinctions exist between the surface locations of the FP and DNA: anionic DNA appears to be submerged into the headgroup and glycerol backbone region of the lipid bilayer, possibly due to favorable electrostatic interactions with the cationic headgroups, whereas the hydrophobic β-sheet FP appears to reside on the surface of the lipid headgroups.

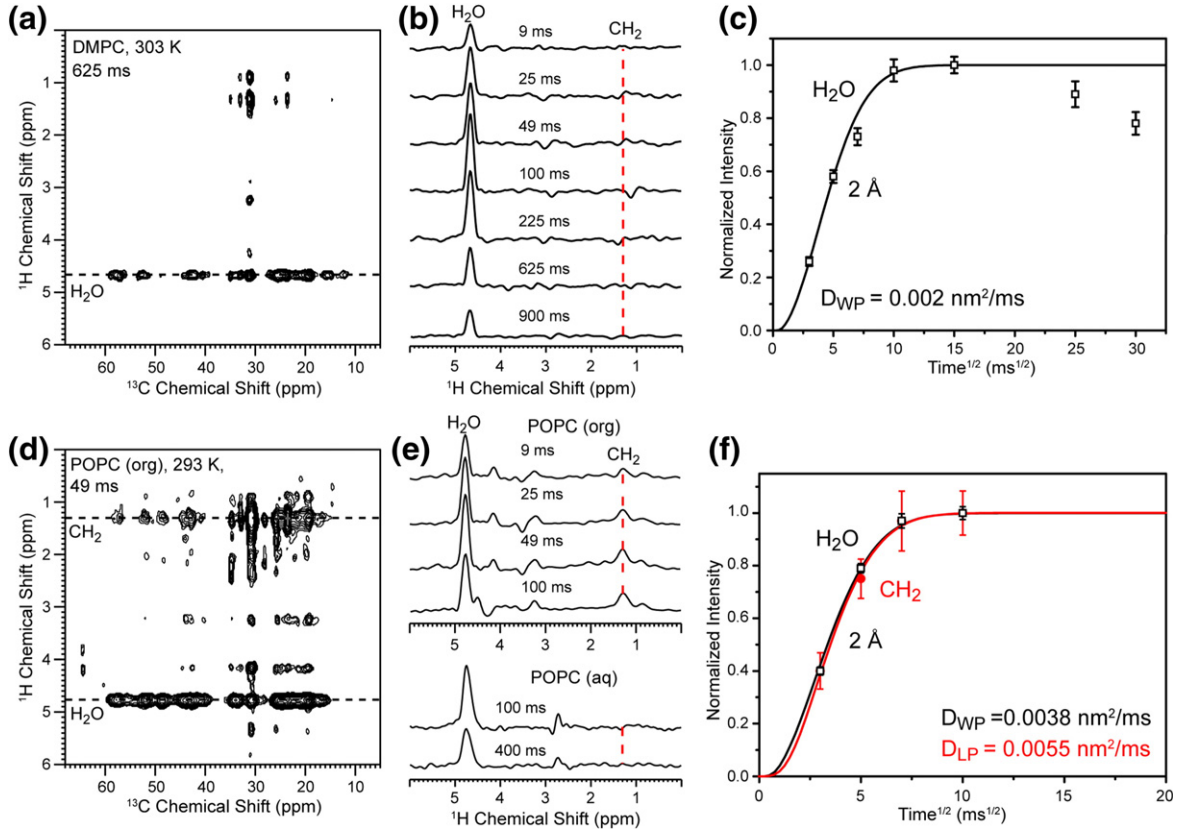

Fig. 5. Depth of insertion of the PIV5 FP obtained from 2D ^{13}C-detected ^{1}H spin diffusion spectra measured in the liquid-crystalline phase. (a) 2D spectrum of DMPC-bound FP(103–132) with a 625-ms ^{1}H mixing time. (b) ^{1}H cross sections as a function of mixing time, obtained as the sum of the C^{α} signals from 39.2 ppm to 60.5 ppm. (c) Buildup curve of the water–peptide cross peak. No lipid CH_2–peptide cross peak was observed. (d) 2D spectrum of the organic POPC-bound FPK4 sample with a 49-ms mixing time. Clear lipid–peptide cross peaks are observed. (e) ^{1}H cross sections as a function of mixing time for the organic POPC/FPK4 sample. For comparison, the cross sections of the aqueous POPC/FPK4 sample are shown at the bottom: no peptide–lipid cross peaks are detected. (f) Water–peptide and lipid–peptide buildup curves of the organic POPC/FPK4 sample.

Similar to the DMPC-bound FP, the aqueous POPC/FPK4 sample did not exhibit any lipid–peptide cross peaks (Fig. 5e). However, the organic POPC/FPK4 sample showed clear lipid–peptide cross peaks (Fig. 5d–f) at mixing times as short as 9 ms and the cross peak intensity buildup with time is well fit to a minimum distance of 2 Å between the acyl chains and the peptide. Thus, not exposing the FP to a large volume of aqueous solution caused the peptide to fully insert into the bilayer. It is reasonable to assume that the FP encounters an aqueous environment during its change from the interior of the globular head in the pre-fusion state to the membrane-anchored state in the extended prehairpin intermediate (Fig. 1a). Thus, we tentatively assign this inserted β-sheet topology, created by the lack of significant aqueous solution, to a kinetically trapped non-equilibrium structure.

Effects of the FP on membrane curvature and hydration

Next, we investigated the curvature and hydration of FP-containing lipid membranes using ^{31}P NMR experiments at physiological temperature. To understand how PIV5 FP affects membrane curvature, we measured static ^{31}P spectra, which are sensitive to the morphology and phase of the lipid membrane.[31,32] Lamellar bilayers show a uniaxial powder pattern with a chemical shift span of ~45 ppm, while high-curvature nonlamellar phases such as small (<50 nm) isotropic vesicles and cubic phases exhibit a narrow peak near the isotropic ^{31}P chemical shift of 0 ppm. The latter is due to the lateral diffusion of lipids over the highly curved surface of the nonlamellar domain. Figure 6a shows the static ^{31}P spectra of various FP-containing membranes. The aqueous POPC sample shows a superposition of the powder pattern with a significant isotropic peak at 2.1 ppm, while the two anionic membranes have negligible isotropic intensity. Under MAS, the ^{31}P spectra (Fig. 6b) resolve two isotropic peaks for the POPC membrane: the nonlamellar lipids resonate at an isotropic shift of 2.2 ppm while the lamellar lipids resonate at −0.9 ppm. Thus, the POPC headgroup conformation differs between the high-curvature isotropic phase and the low-curvature lamellar domain.[33] Based on the ^{31}P MAS intensities, the fraction of the nonlamellar phase is 7–20% of the total membrane and increases with the FPK4 concentration (Fig. S3). In contrast, for the two POPG-containing membranes, the nonlamellar component is less than 1% of the total membrane at P/L = 1:20. Taken together,

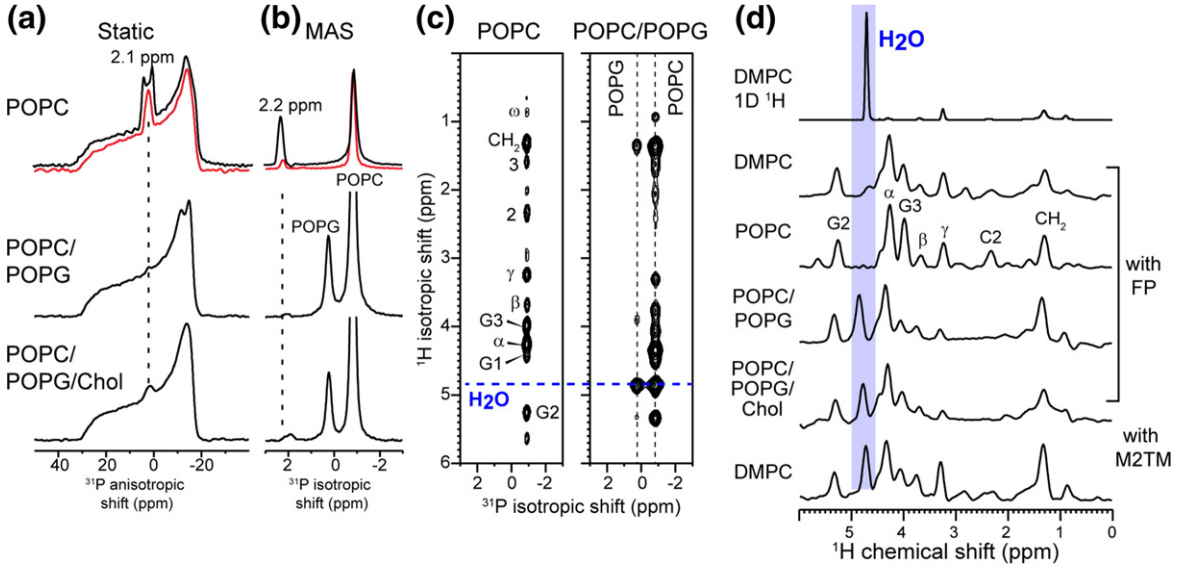

Fig. 6. Peptide–lipid interactions of the PIV5 FP from ^{31}P 1D and 2D spectra. (a) ^{31}P static spectra. FPK4-containing POPC membranes show a narrow isotropic peak in addition to the powder pattern, indicating the coexistence of a high-curvature nonlamellar phase with the lamellar membrane. Black, P/L = 1:15; red, P/L = 1:20. The POPG-containing anionic membranes (P/L = 1:20) have negligible isotropic intensity. (b) ^{31}P MAS spectra. The isotropic chemical shift of POPC is 2.2 ppm for the nonlamellar phase but is −0.9 ppm for the lamellar domain. (c) Representative 2D ^{31}P–^{1}H correlation spectra of FPK4-containing membranes, measured with 225-ms ^{1}H spin diffusion. The POPC membrane does not have a water cross peak while the POPC/POPG membrane does (shaded region). (d) Water ^{1}H cross sections of various lipid membranes obtained from the 2D ^{31}P–^{1}H spectra. POPG-containing membranes have water cross peaks while PC membranes do not. For comparison, the 1D ^{1}H spectrum of pure DMPC is shown at the top, and the ^{1}H cross section of M2TM-containing DMPC is shown at the bottom. All spectra were measured in the liquid-crystalline phase, at 293 K for the POPX (X = C, G) samples and at 303 K for the DMPC samples.

these ^{31}P spectra indicate that the β-sheet FPK4 generates substantial curvature to the neutral membrane whereas the α-helical FPK4 does not disrupt the lamellar order of the anionic membrane.

To investigate whether the lipid headgroups are dehydrated in the presence of bound peptide, as suggested for some fusion intermediates (Fig. 1a),[34] we measured the 2D ^{31}P–^{1}H correlation spectra. Well-hydrated lipid membranes containing exchangeable protons in either the lipid or the protein readily exhibit a water ^{1}H-to-lipid ^{31}P cross peak.[35] Figure 6c and d shows that the two FP-containing anionic membranes have strong water–^{31}P cross peaks; however, the DMPC and aqueous POPC membranes exhibit weak or no water cross peak. Since hydrated but peptide-free PC membranes also do not exhibit a water–^{31}P cross peak due to the lack of exchangeable protons, we used an M2TM-bound DMPC sample as an additional control. Indeed, its 2D spectrum shows a clear water–^{31}P cross peak (Fig. 6d), confirming that, with bound peptides, a hydrated PC membrane manifests a water–^{31}P cross peak. Therefore, the absence or weakness of this water cross peak for the FP-containing DMPC and POPC membranes strongly suggests dehydration of the neutral membrane.

Discussion

Conformational plasticity of the PIV5 FP

Extensive structural studies indicate that the conformation of viral FPs depends sensitively on the environment,[36] but few studies have related the peptide conformation to fusion intermediates. The current work aims to address both the conformational polymorphism of the PIV5 FP and the relation of the multiple conformations to the proposed fusion intermediates. ^{13}C chemical shifts indicate that the PIV5 FP conformation depends critically on the anionic lipid content of the phospholipid bilayer. A predominantly α-helical conformation is found in POPG-containing membranes with and without cholesterol, whereas neutral PC membranes promote a mostly β-strand structure. Other environmental factors examined here, including the P/L ratio, the Lys tag, and the exposure of the proteoliposomes to a large aqueous solution, do not change the secondary structure. However, access to the aqueous solution affected the depth of insertion of the peptide: when the membrane mixture is exposed to a large aqueous solution, the β-sheet peptide equilibrates to a membrane-surface location while, with restricted access to water, the β-sheet peptide is inserted across the lipid bilayer. The disappearance of the inserted β-sheet topology upon exposure to aqueous solution suggests that this topology is likely a non-equilibrium structure; whether or not such a structure is relevant to membrane fusion requires further studies.

NMR chemical shifts at high P/L together with CD data at low P/L indicate that the β-sheet conformation is stable between P/L ratios of 1:100 and 1:13. Since the peptide and lipids were initially codissolved in organic solvents, the β-sheet structure is not due to incomplete solubilization of the peptide before membrane binding but represents the intrinsic structure of the PIV5 FP in zwitterionic PC membranes.

Attenuated total reflection IR data of PIV5 FP showed an α-helical conformation in POPC bilayers at a high P/L of 1:20,[37] in contrast to the current results. Various sample differences may explain these different findings. The peptide construct used in the previous study spanned residues 103–132 and used a GGGW C-terminal tag, while the main construct used in the current study spans residues 103–129 and used a DIOXA-KKKK tag. Moreover, the IR samples were prepared by directly mixing the peptide aqueous solution with the POPC vesicle solution, while the current SSNMR samples were prepared by first mixing the peptide and lipids in organic solvents before switching to the aqueous solution.

The intermediate-timescale motion of the α-helical FP in the anionic membrane precluded direct measurement of the peptide orientation and depth at present. However, this motion rules out an in-plane orientation of the helix, since the large radius of the helix in the membrane plane would result in slow rotational diffusion and rigid-limit spectra.[38,39] We hypothesize that the motion may result from a combination of a tilted orientation and a high oligomeric number of the α-helical peptide. Extensive NMR studies of the influenza M2TM indicate that the four-helix bundle formed by M2TM undergoes fast ($>10^{6}$ s^{-1}) uniaxial diffusion in POPC bilayers at physiological temperature.[25,40,41] Thus, for the PIV5 FP to exhibit slower motion, either the oligomeric state is larger than four or the helix tilt angle is much larger than that of M2TM (~35°). Some support for a high oligomeric number is given by analytical ultracentrifugation data of dodecylphosphocholine (DPC)-bound PIV5 FP, which showed hexamer formation.[37] Indirect support for a large tilt angle is gleaned from the influenza HA FP, which traverses a single leaflet of the bilayer in an oblique orientation.[16] Further experiments are necessary to directly determine the membrane topology of the α-helical PIV5 FP in the anionic lipid bilayer.

Functional relevance of the α-helical and β-sheet conformations

Insights into the possible functional relevance of the α-helical and β-sheet conformations of PIV5 FP

can be gained by correlating the secondary structure with peptide dynamics, depth of insertion, membrane morphology, and membrane hydration. In the zwitterionic PC membrane, the β-sheet FP is immobilized, lies on the membrane surface, induces and stabilizes a high-curvature nonlamellar membrane phase, and dehydrates the membrane surface. The latter two features are the key signatures of the hemifusion intermediate (Fig. 1a). Continuous elastic models of membrane leaflets, molecular dynamics simulations,[10,11] and X-ray diffraction of protein-free membranes[42] all suggested bending, splaying and tilting of the lipid chains, and the significant dehydration of the inter-membrane space in the hemifusion state. The fusion protein is thought to lower the energy barrier for this membrane deformation as well as lower the hydration repulsion, which normally keeps two bilayers separated by 10–20 Å, through its conformational changes.[1,43] While various membrane peptides such as antimicrobial peptides and cell-penetrating peptides can generate membrane curvature for function,[7,8,33,44–46] none of these peptides have yet been found to dehydrate the lipid headgroups.[35,47,48] Thus, the weakness of a ^{31}P–water cross peak for the FP-containing DMPC and POPC membranes is a striking property of the β-sheet FP and suggests that the β-structure may be the relevant conformation for the high-curvature and dehydrated hemifusion intermediate (Fig. 7a). The nonlamellar phase represents only a small fraction (up to about 20%) of the total PC membrane under the experimental conditions used here. This is reasonable: during virus–cell fusion, only regions of the membrane with a high density of the FP should experience enhanced membrane curvature that is necessary for causing the final fusion pore.

Compared to the β-sheet state, the α-helical FP has the signatures of the extended prehairpin state and the post-fusion state. The helix undergoes intermediate-timescale motion, likely due to tilted insertion, and maintains the hydration and lamellar order of the membrane. Both the extended prehairpin and the post-fusion state require the FP to be well inserted into the lipid membrane (Fig. 7b), and the former also implies a lamellar bilayer. The post-fusion state has been thought to involve association of the FP and TM domains, which may be better accomplished by the α-helical than the β-sheet conformation. Analytical ultracentrifugation data indicate that mixtures of helical FP and TM in DPC micelles have a strong propensity to form hexamers.[37] Our tentative assignment of the α-helical FP, which resides in a lamellar membrane, to the post-fusion state contradicts the traditional depiction of the post-fusion state as having high membrane curvature.[10,11] Further experiments are necessary to clarify the membrane morphology of the post-fusion state and the structure of the FP in that state.

The proposed functional relevance of the β-sheet FP may be consistent with the Gly-rich amino acid sequences of the paramyxovirus and other class I viral FPs. Gly has the dichotomy of promoting non-helical structures as well as facilitating intermolecular association of TM helices. Thus, the FP sequences may be particularly well suited to conformational transitions between the helical and non-helical structures, which may be necessary to ensure membrane fusion at the right place and the right time. Mutagenesis of Gly residues in various FPs has led to different results about the fusion activity. Influenza HA FP Gly-to-Ala mutants are less fusogenic than the wild-type peptide,[49] while PIV5 FP Gly-to-Ala mutants have increased fusion activity.[50] The latter was found to result from a lower energy barrier for activating the F protein at a step prior to the extended intermediate and hemifusion.[51] Since it is not known whether these Gly-to-Ala mutants adopt more or less helical structures than the wild-type peptide, it is difficult to

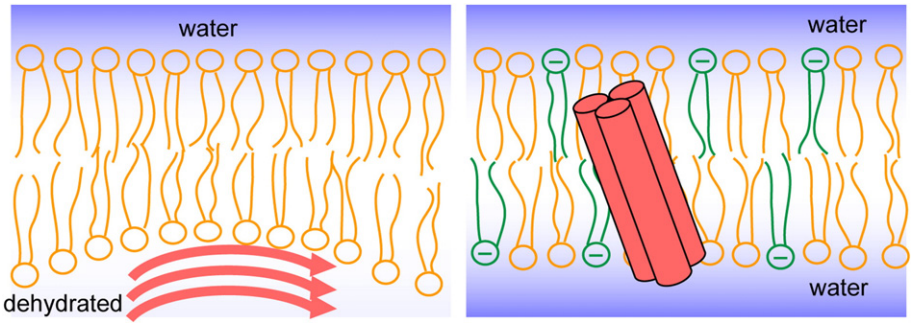

Fig. 7. Schematic models of the membrane-dependent structures of the PIV5 FP. The peptide adopts β-sheet conformation in neutral POPC and DMPC membranes, is oligomerized, resides on the membrane surface, dehydrates the lipid headgroups, and incurs significant membrane curvature. In contrast, in anionic POPC/POPG membranes, the FP adopts an α-helical conformation, undergoes intermediate-timescale motion, and retains the hydration and lamellar order of the membrane. The depicted orientation and oligomeric state of the α-helical peptide are inferred from the dynamics data and require future experimental validation.

use the mutagenesis results to assign the fusogenic secondary structure.

The fact that the nonlamellar-phase-inducing and lipid-dehydrating β-sheet FP exists only in the neutral PC membrane suggests a role for lipids in regulating membrane fusion. The spatial distribution of lipids in eukaryotic membranes is not uniform,[52] with acidic phospholipids mainly existing in the inner leaflet of the plasma membrane.[52] The POPG trigger for the sheet-to-helix conformational change of PIV5 FP suggests the following scenario. After the extended prehairpin intermediate is established, the FP, in the target membrane as an α-helix, may encounter a predominantly neutral region of the membrane, which triggers its change to the β-strand conformation. The β-strand oligomerizes and binds to the membrane surface, in so doing dehydrating the lipid headgroups. At the same time, the intrinsic curvature of the oligomeric β-sheet may increase the membrane curvature (Fig. 7), which reduces the energy barrier for merging the viral and target cell membranes. The FP-induced curvature may augment the curvature caused by lipids with negative spontaneous curvature such as phosphatidylethanolamine. The fluid nature of the cell membrane makes it possible for the transient formation of a neutral or negatively charged area of the membrane surrounding the FP. The amino acid sequence of the FP may further modulate its immediate lipid environment, by causing clustering of certain lipids[53] to promote its own conformational change.

Comparison of PIV5 FP with other class I viral FPs

Extensive spectroscopic studies indicate that the influenza and HIV FPs also exhibit conformational polymorphism but in response to different environmental triggers. For the influenza HA FP, the secondary structure is predominantly α-helical in both detergents[54] and lipid bilayers.[55] However, pH and ionic strength affect the conformation and oligomeric structure: acidic pH promotes a monomeric α-helical conformation whereas high pH and high ionic strength shift the equilibrium to an aggregated β-sheet.[56] The three-dimensional fold of the HA FP is sensitive to the amino acid sequence: a shorter peptide adopts a bent helix structure[16,34] while a longer sequence that contains an additional GxxW segment and two different amino acids near the turn (N12G and E15T) adopts a tight helical hairpin structure.[18] The HIV FP is more polymorphic. Among a large number of environmental factors, P/L and cholesterol content are the most important: high peptide concentration and cholesterol at a level similar to the virus envelope induce β-sheet structure that is partially inserted into the membrane,[19,20,22,57–59] while in detergent micelles or at low peptide concentrations, the HIV FP is mainly α-helical.[17,58] Interestingly, among the various detergents, the negatively charged SDS induced a more ordered α-helical structure for HIV FP than the neutral DPC. Early CD and IR studies of HIV FP in POPG and POPC bilayers also showed that the POPG membrane promotes the α-helical conformation whereas the POPC membrane yielded β-structures at all P/L ratios.[60] Finally, SSNMR data showed that when cholesterol was absent, the POPC/POPG bilayer induced the α-helical conformation.[19] Therefore, HIV and PIV5 FPs appear to share a common conformational dependence on the membrane-surface charge. One difference is that the PIV5 FP helix persists in the mixed POPC/POPG/cholesterol membrane, whereas the HIV FP converts to β-sheet upon the addition of cholesterol, even when the membrane contains anionic lipids.[57]

Despite the different factors for the conformational equilibrium, the common ability of these viral FPs to modulate their structure and depth of insertion indicates that structural plasticity is essential for protein-mediated viral membrane fusion. This plasticity allows the FP to respond to environmental cues to change the local membrane curvature and lipid headgroup hydration at the right place and the right time. Further elucidation of the membrane fusion mechanism will require high-resolution structures of the FP as well as the TM domain and determination of the membrane structure at the site of the FP in different stages of fusion.

Materials and Methods

Peptide and lipids

Peptides corresponding to residues 103–129 or residues 103–132 of the PIV5 F protein (FAGVVIGLAAL GVATAAQVTAAVALVK) were synthesized using Fmoc chemistry by PrimmBiotech (Cambridge, MA). To increase the solubility of the peptide, we added a KKKK tag to the C-terminus of FP(103–129) through a DIOXA linker. The amino acid sequence of PIV5 FP and its comparison with HIV and influenza FPs are shown in Fig. S4. All three FPs show an abundance of small residues, Ala and Gly.[37] We also prepared an untagged FP(103–132) peptide to compare with FPK4(103–129). Two sets of ^{13}C, ^{15}N-labeled residues were used in the current study: G114, V115, A126, and L127 for one sample (GVAL-FPK4) and I108, G109, A112, L113, and V125 (IGALV-FPK4) for the second sample.

Membranes with several different lipid compositions, including DMPC, POPC, POPC/POPG (4:1 molar ratio), and POPC/POPG/cholesterol (4:1:1.5 molar ratio), were prepared. The peptide was dissolved in trifluoroethanol or hexafluoroisopropanol and mixed with lipids in chloroform. The mixture was dried under a stream of nitrogen and lyophilized overnight. The dry mixture was suspended in a pH 7.5 phosphate buffer (10 mM Na_2HPO_4 and NaH_2PO_4,

1 mM ethylenediaminetetraacetic acid, and 1 mM NaN_3), dialyzed for one day, then spun at 55,000 rpm for 4 h at 4 °C to obtain a membrane pellet, which was packed into a 4-mm MAS rotor. These samples are called aqueous samples because of the exposure of the proteoliposomes to large volumes of aqueous solution. For one of the POPC samples, we packed the dry peptide–lipid mixture into the rotor and hydrated it directly with buffer to ~40% hydration (w/w). We call this sample the organic sample. The P/L molar ratio was 1:20 for most samples, 1:15 for the DMPC-bound IGALV-FP without the polar tag, and 1:13 for the organic POPC-bound GVAL-FPK4 sample.

SSNMR experiments

SSNMR spectra were measured at magnetic fields of 9.4 T and 14.1 T using wide-bore Bruker spectrometers operating at ^{1}H Larmor frequencies of 400 MHz and 600 MHz, respectively. We used 4-mm MAS probes tuned to ^{1}H/^{13}C/^{15}N and ^{1}H/^{31}P. ^{13}C chemical shifts were externally referenced to the α-Gly C′ signal at 176.465 ppm on the neat TMS scale, while ^{31}P chemical shifts were referenced to the hydroxyapatite ^{31}P signal at +2.73 ppm on the phosphoric acid scale. ^{13}C chemical shifts were measured in the gel phase of the lipid membranes (243 K or 263 K) to obtain higher sensitivity and avoid dynamic broadening of the peptide signals. Comparison of 1D ^{13}C spectra at low and high temperatures (Fig. 4) indicates that the FP conformation is unaffected by temperature. All other experiments, which measure membrane curvature, hydration, peptide insertion depths, and peptide dynamics, were carried out in the liquid-crystalline phase of the membranes.

Conformation-dependent ^{13}C chemical shifts were measured using 2D ^{13}C–^{13}C correlation experiments with spin diffusion mixing times of 10–20 ms, supplemented with 1D DQ filtered ^{13}C experiments, in which the DQ excitation and reconversion were achieved using the SPC-5 sequence.[61] Most spectra were measured in the gel-phase membrane at 243 K and the MAS rate was typically 7 kHz.

The depth of insertion of FP was measured using the 2D ^{13}C-detected ^{1}H spin diffusion experiment[29] at ambient temperature under 5-kHz MAS. A ^{1}H T_2 filter of 0.4–1.0 ms selected the magnetization of the mobile lipid and water. After ^{1}H chemical shift evolution, a mixing time (t_m) of 9–900 ms was applied to transfer ^{1}H polarization from lipids and water to the peptide. The result of this transfer was detected through the ^{13}C signals of the peptide. Strong cross peaks between lipid CH_2 and peptide ^{13}C signals indicate peptide insertion into the center of the membrane. Cross peak intensities as a function of mixing time were corrected for ^{1}H T_1 relaxation and normalized with respect to the maximum H_2O or CH_2 intensity. The buildup curves were simulated as described before.[6,29] A lattice spacing of 2 Å was used. Diffusion coefficients of 0.012 nm^2/ms and 0.30 nm^2/ms were used for the lipid (D_L) and peptide (D_P), respectively. For the DMPC sample, the water buildup curve was fit using an interfacial diffusion coefficient (D_{WP}) of 0.002 nm^2/ms, corresponding to a transfer rate of 50 Hz. For the organic POPC membrane, the best fits of CH_2 and H_2O data were obtained using a lipid–peptide diffusion coefficient (D_{LP}) of 0.0055 nm^2/ms (transfer rate, 138 Hz) and a D_{WP} of 0.0038 nm^2/ms (transfer rate, 95 Hz), respectively.

2D ^{31}P–^{1}H correlation experiment analogous to the ^{13}C–^{1}H spin diffusion experiment[35] was conducted to determine the hydration of the membrane surface through the water ^{1}H–^{31}P cross peak. The spectra were measured at 293 K for POPC membranes and 303 K for DMPC membranes under 4- or 5-kHz MAS. The ^{1}H–^{31}P CP contact time was 3 ms.

The dynamics of FP in lipid bilayers was investigated using the ^{13}C–^{1}H dipolar-chemical-shift correlation experiment under 4-kHz MAS at 303 K. MREV-8[62] was used for ^{1}H homonuclear decoupling during the evolution period. The MREV-8 ^{1}H pulse length was 4 μs, corresponding to a flip angle of 105°. For the POPC-bound GVAL-FPK4, significant lipid–peptide resonance overlap was present. Thus, we conducted a DQ filtered dipolar-chemical-shift correlation experiment,[63] which suppressed the lipid natural abundance ^{13}C signals. The experiment was carried out under 4.5-kHz MAS at 293 K. The time-domain dipolar dephasing was fit to obtain the apparent couplings, which were divided by the theoretical scaling factor of 0.47 to obtain the true couplings. A rigid-limit coupling of 22.7 kHz was used to calculate the order parameters.

CD experiments

For the CD experiments, membrane samples were prepared by first mixing the peptide and lipids in trifluoroethanol and chloroform, lyophilizing, then hydrating the mixture in pH 7.5 phosphate buffer. The final peptide concentration was 0.1 mg/ml. Two P/L molar ratios, 1:100 and 1:20, were used. The proteoliposome solutions were extruded though 100-nm polycarbonate filters (Avanti Polar Lipids) to obtain large unilamellar vesicles. The extrusion and CD experiments were carried out at room temperature for the POPX (X=C, G) membranes and 30 °C for the DMPC samples. CD spectra were measured on a Jasco J-715 CD spectropolarimeter. Three scans were averaged for each spectrum using a quartz cuvette with a 0.1-cm path length. For each membrane composition, peptide-free large unilamellar vesicles were measured as controls and their signals were subtracted from the spectra of the peptide-containing samples. The contents of secondary structures were estimated using the CDPro software package†.

Acknowledgement

This work is funded by the National Institutes of Health grant GM066976 to M.H.

Supplementary Data

Supplementary data to this article can be found online at http://dx.doi.org/10.1016/j.jmb.2012.11.027

Received 24 July 2012;
Received in revised form 6 November 2012;
Accepted 20 November 2012
Available online 23 November 2012

Keywords:
viral membrane fusion;
magic angle spinning;
conformational plasticity;
membrane dehydration;
intermediate-timescale motion

† http://lamar.colostate.edu/~sreeram/CDPro/main.html

Abbreviations used:
PC, phosphocholine; POPG, palmitoyloleoylphosphatidylglycerol; POPC, palmitoyloleoylphosphatidylcholine; DMPC, dimyristoylphosphatidylcholine; DPC, dodecylphosphocholine; FP, fusion peptide; PIV5, parainfluenza virus 5; CP, cross-polarization; HIV, human immunodeficiency virus; IR, infrared; MAS, magic angle spinning; TM, transmembrane; DQ, double-quantum; M2TM, M2 transmembrane peptide; 2D, two-dimensional; 1D, one-dimensional; SSNMR, solid-state NMR.

References

1. Harrison, S. C. (2008). Viral membrane fusion. *Nat. Struct. Mol. Biol.* **15**, 690–698.
2. Lamb, R. A. & Jardetzky, T. S. (2007). Structural basis of viral invasion: lessons from paramyxovirus F. *Curr. Opin. Struct. Biol.* **17**, 427–436.
3. Rossman, J. S. & Lamb, R. A. (2011). Influenza virus assembly and budding. *Virology*, **411**, 229–236.
4. Nayak, D. P., Hui, E. K. & Barman, S. (2004). Assembly and budding of influenza virus. *Virus Res.* **106**, 147–165.
5. Brogden, K. A. (2005). Antimicrobial peptides: pore formers or metabolic inhibitors in bacteria? *Nat. Rev., Microbiol.* **3**, 238–250.
6. Mani, R., Cady, S. D., Tang, M., Waring, A. J., Lehrer, R. I. & Hong, M. (2006). Membrane-dependent oligomeric structure and pore formation of a β-hairpin antimicrobial peptide in lipid bilayers from solid-state NMR. *Proc. Natl Acad. Sci. USA*, **103**, 16242–16247.
7. Tang, M., Waring, A. J. & Hong, M. (2007). Phosphate-mediated arginine insertion into lipid membranes and pore formation by a cationic membrane peptide from solid-state NMR. *J. Am. Chem. Soc.* **129**, 11438–11446.
8. Mishra, A., Gordon, V. D., Yang, L., Coridan, R. & Wong, G. C. L. (2008). HIV TAT forms pores in membranes by inducing saddle-splay curvature: potential role of bidentate hydrogen bonding. *Angew. Chem., Int. Ed. Engl.* **47**, 2986–2989.
9. Schmidt, N. W., Mishra, A., Lai, G. H., Davis, M., Sanders, L. K., Tran, D. *et al.* (2011). Criterion for amino acid composition of defensins and antimicrobial peptides based on geometry of membrane destabilization. *J. Am. Chem. Soc.* **133**, 6720–6727.
10. Chernomordik, L. V. & Kozlov, M. M. (2005). Membrane hemifusion: crossing a chasm in two leaps. *Cell*, **123**, 375–382.
11. Chernomordik, L. V. & Kozlov, M. M. (2008). Mechanics of membrane fusion. *Nat. Struct. Mol. Biol.* **15**, 675–683.
12. Connolly, S. A., Leser, G. P., Yin, H. S., Jardetzky, T. S. & Lamb, R. A. (2006). Refolding of a paramyxovirus F protein from prefusion to postfusion conformations observed by liposome binding and electron microscopy. *Proc. Natl Acad. Sci. USA*, **103**, 17903–17908.
13. Yin, H. S., Paterson, R. G., Wen, X., Lamb, R. A. & Jardetzky, T. S. (2005). Structure of the uncleaved ectodomain of the paramyxovirus (hPIV3) fusion protein. *Proc. Natl Acad. Sci. USA*, **102**, 9288–9293.
14. Yin, H. S., Wen, X., Paterson, R. G., Lamb, R. A. & Jardetzky, T. S. (2006). Structure of the parainfluenza virus 5 F protein in its metastable, prefusion conformation. *Nature*, **439**, 38–44.
15. Tamm, L. K., Crane, J. & Kiessling, V. (2003). Membrane fusion: a structural perspective on the interplay of lipids and proteins. *Curr. Opin. Struct. Biol.* **13**, 453–466.
16. Han, X., Bushweller, J. H., Cafiso, D. S. & Tamm, L. K. (2001). Membrane structure and fusion-triggering conformational change of the fusion domain from influenza hemagglutinin. *Nat. Struct. Biol.* **8**, 715–720.
17. Jaroniec, C. P., Kaufman, J. D., Stahl, S. J., Viard, M., Blumenthal, R., Wingfield, P. T. & Bax, A. (2005). Structure and dynamics of micelle-associated human immunodeficiency virus gp41 fusion domain. *Biochemistry*, **44**, 16167–16180.
18. Lorieau, J. L., Louis, J. M. & Bax, A. (2010). The complete influenza hemagglutinin fusion domain adopts a tight helical hairpin arrangement at the lipid:water interface. *Proc. Natl Acad. Sci. USA*, **107**, 11341–11346.
19. Yang, J., Gabrys, C. M. & Weliky, D. P. (2001). Solid-state nuclear magnetic resonance evidence for an extended beta strand conformation of the membrane-bound HIV-1 fusion peptide. *Biochemistry*, **40**, 8126–8137.
20. Yang, J. & Weliky, D. P. (2003). Solid-state nuclear magnetic resonance evidence for parallel and antiparallel strand arrangements in the membrane-associated HIV-1 fusion peptide. *Biochemistry*, **42**, 11879–11890.
21. Yang, J., Prorok, M., Castellino, F. J. & Weliky, D. P. (2004). Oligomeric β-structure of the membrane-bound HIV-1 fusion peptide formed from soluble monomers. *Biophys. J.* **87**, 1951–1963.
22. Qiang, W., Sun, Y. & Weliky, D. P. (2009). A strong correlation between fusogenicity and membrane insertion depth of the HIV fusion peptide. *Proc. Natl Acad. Sci. USA*, **106**, 15314–15319.
23. Han, X. & Tamm, L. K. (2000). A host-guest system to study structure–function relationships of membrane fusion peptides. *Proc. Natl Acad. Sci. USA*, **97**, 13097–13102.
24. deAzevedo, E. R., Saalwachter, K., Pascui, O., de Souza, A. A., Bonagamba, T. J. & Reichert, D. (2008). Intermediate motions as studied by solid-state separated local field NMR experiments. *J. Chem. Phys.* **128**, 104505.
25. Cady, S. D., Goodman, C., Tatko, C., DeGrado, W. F. & Hong, M. (2007). Determining the orientation of uniaxially rotating membrane proteins using unoriented samples: a ^{2}H, ^{13}C, and ^{15}N solid-state NMR investigation of the dynamics and orientation of a transmembrane helical bundle. *J. Am. Chem. Soc.* **129**, 5719–5729.

26. Warschawski, D. E., Gross, J. D. & Griffin, R. G. (1997). Dynamics of gramicidin A deduced from high-resolution magic-angle spinning NMR. *Biophys. J.* **72**, WP440.
27. Su, Y., Waring, A. J., Ruchala, P. & Hong, M. (2010). Membrane-bound dynamic structure of an arginine-rich cell-penetrating peptide, the protein transduction domain of HIV TAT, from solid-state NMR. *Biochemistry*, **49**, 6009–6020.
28. Luo, W., Cady, S. D. & Hong, M. (2009). Immobilization of the influenza A M2 transmembrane peptide in virus-envelope mimetic lipid membranes: a solid-state NMR investigation. *Biochemistry*, **48**, 6361–6368.
29. Huster, D., Yao, X. L. & Hong, M. (2002). Membrane protein topology probed by ^{1}H spin diffusion from lipids using solid-state NMR spectroscopy. *J. Am. Chem. Soc.* **124**, 874–883.
30. Radler, J. O., Koltover, I., Salditt, T. & Safinya, C. R. (1997). Structure of DNA–cationic liposome complexes: DNA intercalation in multilamellar membranes in distinct interhelical packing regimes. *Science*, **275**, 810–814.
31. Cullis, P. R. & Kruijff, B. D. (1979). Lipid polymorphism and the functional roles of lipids in biological membranes. *Biochim. Biophys. Acta*, **559**, 399–420.
32. Seelig, J. (1978). ^{31}P NMR and the head group structure of phospholipids in membranes. *Biochim. Biophys. Acta*, **515**, 105–140.
33. Wang, T., Cady, S. D. & Hong, M. (2012). NMR determination of protein partitioning into membrane domains with different curvatures and application to the influenza M2 peptide. *Biophys. J.* **102**, 787–794.
34. Tamm, L. K. (2003). Hypothesis: spring-loaded boomerang mechanism of influenza hemagglutinin-mediated membrane fusion. *Biochim. Biophys. Acta*, **1614**, 14–23.
35. Doherty, T. & Hong, M. (2009). 2D ^{1}H–^{31}P solid-state NMR studies of the dependence of inter-bilayer water dynamics on lipid headgroup structure and membrane peptides. *J. Magn. Reson.* **196**, 39–47.
36. Hong, M., Zhang, Y. & Hu, F. (2012). Membrane protein structure and dynamics from NMR spectroscopy. *Annu. Rev. Phys. Chem.* **63**, 1–24.
37. Donald, J. E., Zhang, Y., Fiorin, G., Carnevale, V., Slochower, D. R., Gai, F. *et al.* (2011). Transmembrane orientation and possible role of the fusogenic peptide from parainfluenza virus 5 (PIV5) in promoting fusion. *Proc. Natl Acad. Sci. USA*, **108**, 3958–3963.
38. Saffman, P. G. & Delbruck, M. (1975). Brownian motion in biological membranes. *Proc. Natl Acad. Sci. USA*, **72**, 3111–3113.
39. Aisenbrey, C. & Bechinger, B. (2004). Investigations of polypeptide rotational diffusion in aligned membranes by ^{2}H and ^{15}N solid-state NMR spectroscopy. *J. Am. Chem. Soc.* **126**, 16676–16683.
40. Wang, J., Kim, S., Kovacs, F. & Cross, T. A. (2001). Structure of the transmembrane region of the M2 protein H^{+} channel. *Protein Sci.* **10**, 2241–2250.
41. Cady, S. D. & Hong, M. (2009). Effects of amantadine binding on the dynamics of bilayer-bound influenza A M2 transmembrane peptide studied by NMR relaxation. *J. Biomol. NMR*, **45**, 185–196.
42. Yang, L. & Huang, H. W. (2002). Observation of a membrane fusion intermediate structure. *Science*, **297**, 1877–1879.
43. Rand, R. P. & Parsegian, V. A. (1989). Hydration forces between phospholipid bilayers. *Biochim. Biophys. Acta*, **988**, 351–376.
44. Marasinghe, P. A. B., Buffy, J. J., Schmidt-Rohr, K. & Hong, M. (2005). Membrane curvature change induced by an antimicrobial peptide detected by ^{31}P exchange NMR. *J. Phys. Chem. B*, **109**, 22036–22044.
45. Cady, S. D., Wang, T. & Hong, M. (2011). Membrane-dependent effects of a cytoplasmic helix on the structure and drug binding of the influenza virus M2 protein. *J. Am. Chem. Soc.* **133**, 11572–11579.
46. Schmidt, N., Mishra, A., Lai, G. H. & Wong, G. C. (2010). Arginine-rich cell-penetrating peptides. *FEBS Lett.* **584**, 1806–1813.
47. Li, S., Su, Y., Luo, W. & Hong, M. (2010). Water–protein interactions of an arginine-rich membrane peptide in lipid bilayers investigated by solid-state nuclear magnetic resonance spectroscopy. *J. Phys. Chem. B*, **114**, 4063–4069.
48. Luo, W. & Hong, M. (2010). Conformational changes of an ion channel membrane protein detected through water–protein interactions using solid-state NMR spectroscopy. *J. Am. Chem. Soc.* **132**, 2378–2384.
49. Steinhauer, D. A., Wharton, S. A., Skehel, J. J. & Wiley, D. C. (1995). Studies of the membrane fusion activities of fusion peptide mutants of influenza virus hemagglutinin. *J. Virol.* **69**, 6643–6651.
50. Horvath, C. M. & Lamb, R. A. (1992). Studies on the fusion peptide of a paramyxovirus fusion glycoprotein: roles of conserved residues in cell fusion. *J. Virol.* **66**, 2443–2455.
51. Russell, C. J., Jardetzky, T. S. & Lamb, R. A. (2004). Conserved glycine residues in the fusion peptide of the paramyxovirus fusion protein regulate activation of the native state. *J. Virol.* **78**, 13727–13742.
52. van Meer, G., Voelker, D. R. & Feigenson, G. W. (2008). Membrane lipids: where they are and how they behave. *Nat. Rev., Mol. Cell Biol.* **9**, 112–124.
53. Epand, R. F., Maloy, W. L., Ramamoorthy, A. & Epand, R. M. (2010). Probing the "charge cluster mechanism" in amphipathic helical cationic antimicrobial peptides. *Biochemistry*, **49**, 4076–4084.
54. Lai, A. L., Park, H., White, J. M. & Tamm, L. K. (2006). Fusion peptide of influenza hemagglutinin requires a fixed angle boomerang structure for activity. *J. Biol. Chem.* **281**, 5760–5770.
55. Sun, Y. & Weliky, D. P. (2009). ^{13}C–^{13}C correlation spectroscopy of membrane-associated influenza virus fusion peptide strongly supports a helix–turn–helix motif and two turn conformations. *J. Am. Chem. Soc.* **131**, 13228–13229.
56. Han, X. & Tamm, L. K. (2000). pH-dependent self-association of influenza hemagglutinin fusion peptides in lipid bilayers. *J. Mol. Biol.* **304**, 953–965.
57. Lai, A. L., Moorthy, A. E., Li, Y. & Tamm, L. K. (2012). Fusion activity of HIV gp41 fusion domain is related to its secondary structure and depth of membrane insertion in a cholesterol-dependent fashion. *J. Mol. Biol.* **418**, 3–15.

58. Li, Y. & Tamm, L. K. (2007). Structure and plasticity of the human immunodeficiency virus gp41 fusion domain in lipid micelles and bilayers. *Biophys. J.* **93**, 876–885.
59. Nieva, J. L., Nir, S., Muga, A., Goñi, F. M. & Wilschut, J. (1994). Interaction of the HIV-1 fusion peptide with phospholipid vesicles: different structural requirements for fusion and leakage. *Biochemistry*, **33**, 3201–3209.
60. Rafalski, M., Lear, J. D. & DeGrado, W. F. (1990). Phospholipid interactions of synthetic peptides representing the N-terminus of HIV gp41. *Biochemistry*, **29**, 7917–7922.
61. Hohwy, M., Jakobsen, H. J., Eden, M., Levitt, M. H. & Nielsen, N. C. (1998). Broadband dipolar recoupling in the nuclear magnetic resonance of rotating solids: a compensated C7 pulse sequence. *J. Chem. Phys.* **108**, 2686–2694.
62. Munowitz, M., Aue, W. P. & Griffin, R. G. (1982). Two-dimensional separation of dipolar and scaled isotropic chemical shift interactions in magic angle NMR spectra. *J. Chem. Phys.* **77**, 1686–1689.
63. Huster, D., Xiao, L. S. & Hong, M. (2001). Solid-state NMR investigation of the dynamics of colicin Ia channel-forming domain. *Biochemistry*, **40**, 7662–7674.

Supporting Information

Membrane-Dependent Conformation, Dynamics, and Lipid Interactions of the Fusion Peptide of the Paramyxovirus PIV5 From Solid-State NMR

Hongwei Yao and Mei Hong*

Department of Chemistry, Iowa State University, Ames, IA 50011

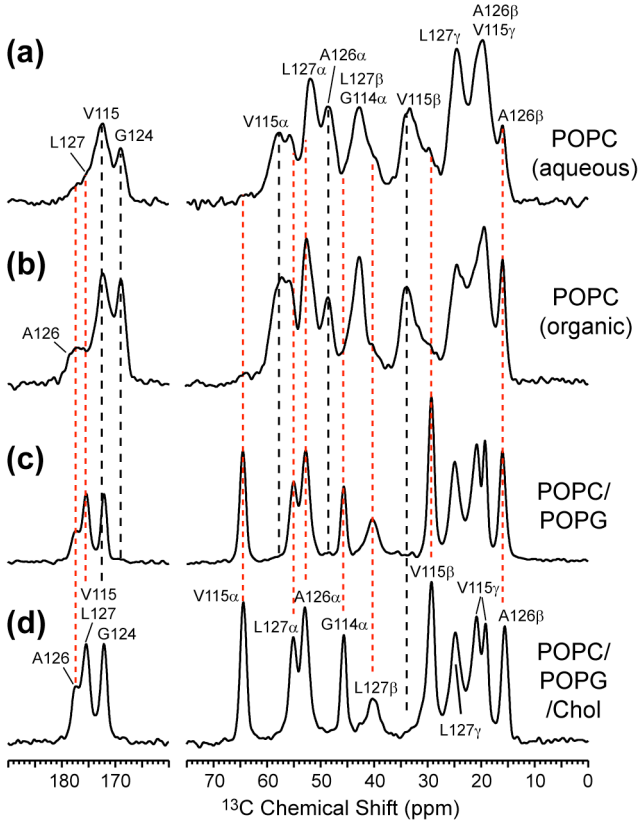

Figure S1. 1D ^{13}C double-quantum filtered spectra of GVAL-FPK4 in various lipid membranes, showing the conformational difference of the peptide on the membrane surface charge. (a) The aqueous POPC sample. (b) The organic POPC sample. (c) The POPC/POPG (4:1) sample. (d) The POPC/POPG/cholesterol (4:1:1.5) sample. Red and black dashed lines guide the eye for α-helical and β-sheet chemical shifts, respectively. The spectra were measured at 243 K.

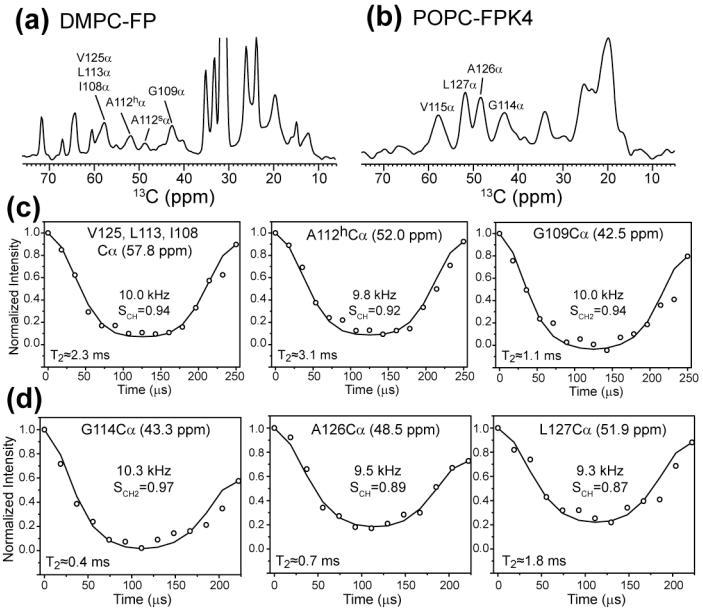

Figure S2. ^{13}C-^{1}H order parameters of the PIV5 fusion peptide in liquid-crystalline DMPC bilayers (a, c) and POPC bilayers (b, d). (a) ^{13}C dimension of the 2D DIPSHIFT spectrum of FP(103-132) in DMPC bilayers, measured under 4 kHz MAS at 303 K. (b) ^{13}C dimension of the DQ filtered DIPSHIFT spectrum of FPK4(103-129) in POPC bilayers, in which the lipid ^{13}C signals are removed. The spectrum was measured under 4.5 kHz MAS at 293 K. (c) Selected Cα-Hα dipolar dephasing curves of DMPC-bound FP. (d) Selected Cα-Hα dipolar dephasing curves of POPC-bound FPK4. The order parameters and the effective T_2 relaxation times are indicated in each panel.

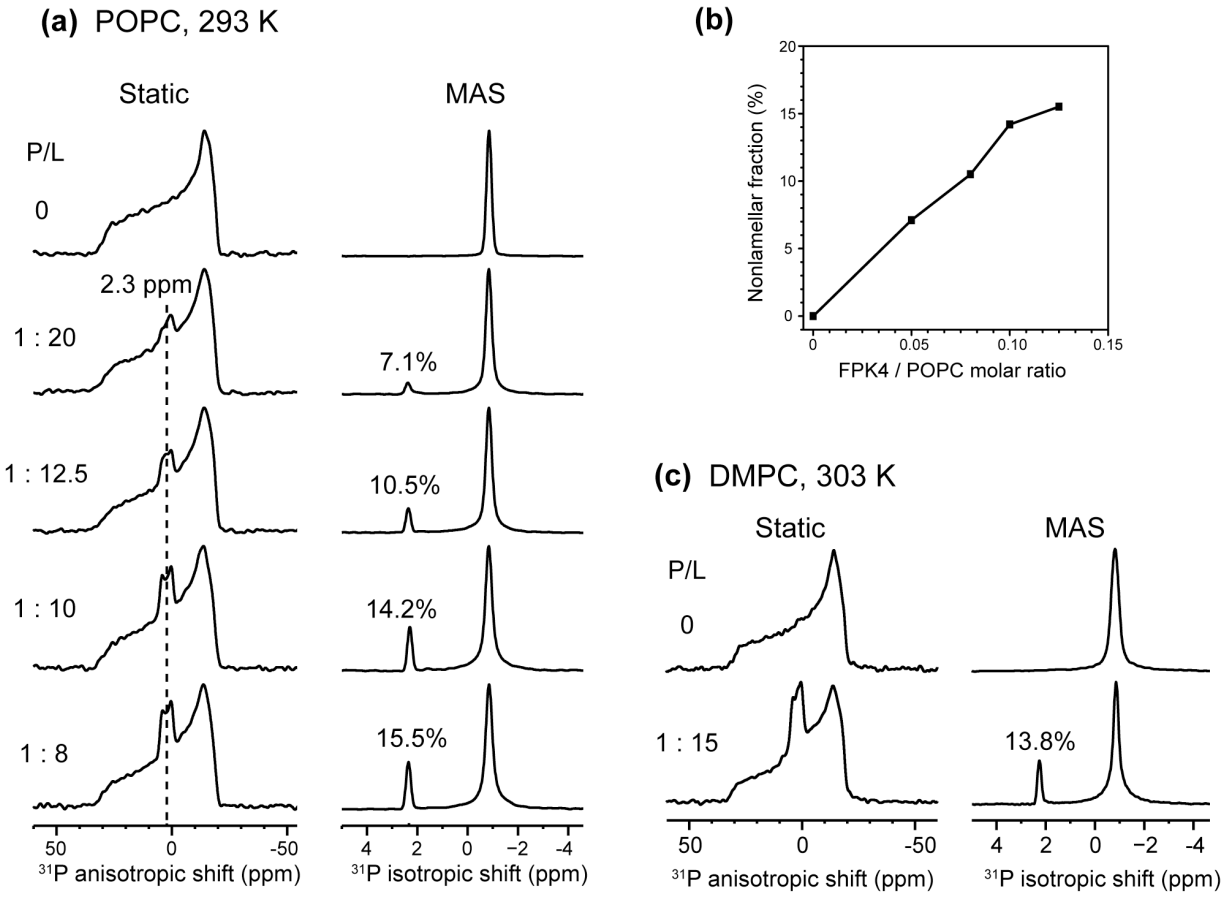

Figure S3. Nonlamellar phase generated by FPK4 to zwitterionic phosphatidylcholine membranes. (a) Static (left) and MAS (right) ^{31}P spectra of POPC membrane at 293 K as a function of FPK4 peptide/lipid molar ratio (P/L). Peptide-free control membrane does not have a nonlamellar peak. Increasing FPK4 concentration caused increasing amounts of the nonlamellar ^{31}P peak at 2.3 ppm. Therefore, the spectra confirm that FPK4 reproducibly causes a high-curvature phase to the POPC membrane. (b) Percentage of nonlamellar phase as a function of P/L for the POPC membrane. (c) Static and MAS ^{31}P spectra of the DMPC membrane without and with FPK4. FPK4 causes the same isotropic phase, as seen by the isotropic peak in the static ^{31}P spectrum and a 2.3-ppm isotropic peak in the MAS spectrum, which differs from the lamellar isotropic chemical shift of -0.9 ppm.

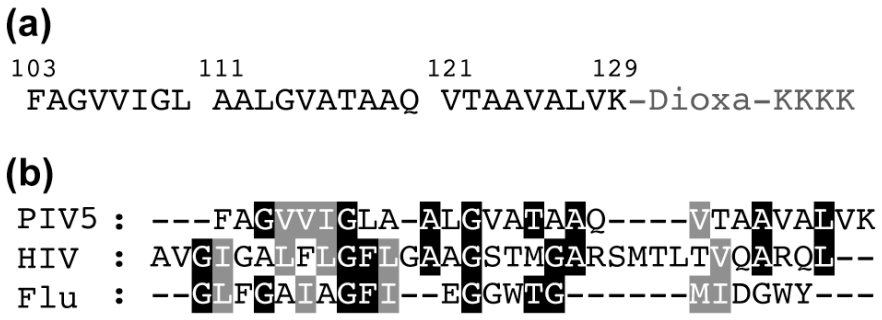

Figure S4. Amino acid sequences of three class I fusion peptides. (a) PIV5 FP with the DIOXA-KKKK tag. (b) Sequence alignment of PIV5, HIV, and influenza fusion peptides.

Table S1: Conformation distribution of the fusion peptide in different membranes from the relative intensities of Cα-Cβ or Cβ-Cγ cross peaks [a].

Membrane & Peptide	Residue	α-helical intensity	β-Sheet intensity
DMPC	A112	53%	47%
POPC	V115	24%	76%
	A126	51%	49%
	L127	54%	46%

[a]: For V115, the percentages were obtained from the Cβ-Cγ cross peak intensity, while for all other residues the percentages were obtained from the Cα-Cβ cross peaks.

Table S2: Conformation distribution of the PIV5 FP in different membranes and P/L ratios based on CD spectra. The percentages have an estimated uncertainty of 10%.

Membrane	P/L	α-helix	β-Sheet	Coil/Turn
DMPC	1 : 100	34%	21%	45%
	1 : 20	26%	29%	45%
POPC	1 : 100	34%	12%	54%
	1 : 20	25%	21%	54%
POPC : POPG (4 : 1)	1 : 100	76%	0%	24%
POPC : POPG : cholesterol (4 : 1 : 1.5)	1 : 100	72%	2%	26%

Table S3: C-H order parameters of IGALV-FP in DMPC bilayers and GVAL-FPK4 in POPC bilayers.

	Chemical Shift (ppm)	S_{CH}
G114Cα	43.3	0.97±0.05
A126Cα	48.5	0.89±0.05
L127Cα	51.9	0.87±0.04
A112Cα	52.0	0.92±0.04
V123Cα L113Cα I108Cα	57.8	0.94±0.04
G109Cα	42.5	0.94±0.06